Title

Spectral and photochemical diversity of tandem cysteine cyanobacterial phytochromes

Journal

Journal of Biological Chemistry, 295(19)

ISSN

0021-9258

Authors

Song, Ji-Young

Lee, Ha Yong

Yang, Hee Wook

et al.

Publication Date

2020-05-01

DOI

10.1074/jbc.ra120.012950

Spectral and photochemical diversity of tandem cysteine cyanobacterial phytochromes

Received for publication, February 6, 2020, and in revised form, March 13, 2020 Published, Papers in Press, March 17, 2020, DOI 10.1074/jbc.RA120.012950

Ji-Young Song[‡1], Ha Yong Lee[‡1], Hee Wook Yang[‡], Ji-Joon Song[§], J. Clark Lagarias[¶2], and Youn-Il Park[‡3]

From the [‡]Department of Biological Sciences, Chungnam National University, Daejeon 34134, Korea, the [§]Department of Biological Science and KI for the BioCentury, Korea Advanced Institute of Science and Technology, Daejeon 34141, Korea, and the [¶]Department of Molecular and Cellular Biology, University of California Davis, Davis, California 95616

Edited by Joseph M. Jez

The atypical trichromatic cyanobacterial phytochrome *Np*TP1 from *Nostoc punctiforme* ATCC 29133 is a linear tetrapyrrole (bilin)-binding photoreceptor protein that possesses tandem-cysteine residues responsible for shifting its light-sensing maximum to the violet spectral region. Using bioinformatics and phylogenetic analyses, here we established that tandem-cysteine cyanobacterial phytochromes (TCCPs) compose a well-supported monophyletic phytochrome lineage distinct from prototypical red/far-red cyanobacterial phytochromes. To investigate the light-sensing diversity of this family, we compared the spectroscopic properties of *Np*TP1 (here renamed *Np*TCCP) with those of three phylogenetically diverged TCCPs identified in the draft genomes of *Tolypothrix* sp. PCC7910, *Scytonema* sp. PCC10023, and *Gloeocapsa* sp. PCC7513. Recombinant photosensory core modules of *To*TCCP, *Sc*TCCP, and *Gl*TCCP exhibited violet-blue–absorbing dark-states consistent with dual thioether-linked phycocyanobilin (PCB) chromophores. Photoexcitation generated singly-linked photoproduct mixtures with variable ratios of yellow-orange and red-absorbing species. The photoproduct ratio was strongly influenced by pH and by mutagenesis of TCCP- and phytochrome-specific signature residues. Our experiments support the conclusion that both photoproduct species possess protonated 15*E* bilin chromophores, but differ in the ionization state of the noncanonical "second" cysteine sulfhydryl group. We found that the ionization state of this and other residues influences subsequent conformational change and downstream signal transmission. We also show that tandem-cysteine phytochromes present in eukaryotes possess similar amino acid substitutions within their chromophore-binding pocket, which tune their spectral properties in an analogous fashion. Taken together, our findings provide a roadmap for tailoring the wavelength specificity of plant phytochromes to optimize plant performance in diverse natural and artificial light environments.

Phytochromes are linear tetrapyrrole (bilin)-based photoreceptors widely distributed in bacteria, algae, fungi, diatoms, and land plants that function as photoswitches to optimize photosynthesis, regulate growth and development and/or entrain behavior with the diurnal light-dark cycle (1–4). Phytochromes possess a conserved multidomain N-terminal photosensory core module (PCM)[4] consisting of PAS (Period/Arnt/Single-minded), GAF (cGMP phosphodiesterase/Adenylyl cyclase/FhlA), and PHY (phytochrome-specific) domains associated with variable C-terminal output modules, the most prevalent functioning as two-component histidine kinases. Prototypical phytochromes transduce red (R) and far-red (FR) light signals via reversible photointerconversion between R-absorbing Pr and FR-absorbing Pfr states (2). Light absorption by phytochromes triggers photoisomerization of the 15,16-double bond of their bilin chromophores (5, 6) that initiates changes in the output module structure to promote downstream signal transduction.

Despite the well-conserved PCM architecture of phytochromes from bacteria to land plants, various lineages have undergone evolutionary changes for sensing shorter wavelengths of light. Small spectral variation is mostly attributed to differences in bilin chromophore composition. Phytochromes leverage three bilin chromophore precursors, *i.e.* biliverdin (BV) and the more reduced phytobilins, phycocyanobilin (PCB), and phytochromobilin (PΦB), which afford modest spectral tuning within the R and FR regions (7). Phytochrome chromophores are thioether linked to conserved cysteine (Cys)

This work was supported by Next-Generation BioGreen 21 Program, Rural Development Administration Grant PJ013118, KIST Open Research Program Grant 2E27512-17-122, the Collaborative Genome Program funded by Ministry of Oceans and Fisheries Grant 20180430, Korea (to Y.-I. P.), and National Institutes of Health Grant R01 GM068552, United States Department of Agriculture National Institute of Food and Agriculture Hatch project number CA-D*-MCB-4126-H, and Chemical Sciences, Geosciences, and the Biosciences Division, Office of Basic Energy Sciences, Office of Science, United States Department of Energy Grant DE-FG02-09ER16117 (to J. C. L.). The authors declare that they have no conflicts of interest with the contents of this article. The content is solely the responsibility of the authors and does not necessarily represent the official views of the National Institutes of Health.

This article contains Data File S1, Figs. S1–S9, and Table S1.

[1] Both authors contributed equally to this work.

[2] To whom correspondence may be addressed. Tel.: 530-752-1865; Fax: 530-752-3085l; E-mail: jclagarias@ucdavis.edu.

[3] To whom correspondence may be addressed. Tel.: 82-42-8215493; Fax: 82-42-8229690; E-mail: yipark@cnu.ac.kr.

[4] The abbreviations used are: PCM, photosensory core module; BphP, bacterial phytochrome; BV, biliverdin; CBCRs, cyanobacteriochromes; Cph, cyanobacterial phytochrome; GAF, cGMP phosphodiesterase/adenylyl cyclase/FhlA domain; PAS, period/Arnt/single-minded domain; PCB, phycocyanobilin; PΦB, phytochromobilin; PHY, phytochrome-specific domain; VB, violet-blue; TCCPs, tandem cysteine cyanobacterial phytochromes; TCEP, tandem cysteine eukaryotic phytochrome; color codes are near-UV (U), 300–394 nm; violet (V), 395–410 nm; blue (B), 411–485 nm; teal (T), 486–514 nm; green (G), 515–569 nm; yellow (Y), 570–585 nm; orange (O), 586–614 nm; red (R), 615–685 nm; far-red (FR), 685–760 nm; near-IR, 761–1000 nm.

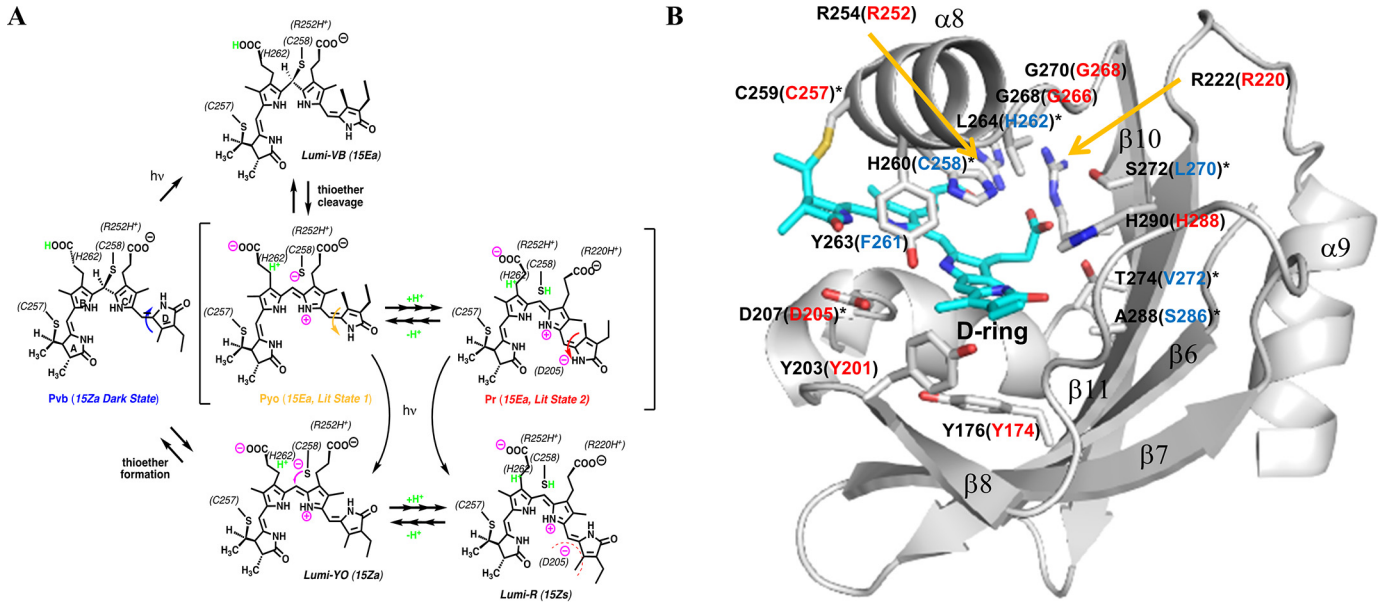

Figure 1. Proposed TCCP photocycle and SyCph1 GAF domain structure labeled with chromophore-containing signature residues. *A*, proposed photocycle. TCCP dark-states absorb violet-to-blue light due to two thioether linkages to the PCB chromophore (15). Light absorption by the ^{15Z}Pvb "dark-state" triggers ultrafast isomerization of the 15*Z* double bond of the doubly-linked PCB chromophore that destabilizes the thioether linkage at C10 to generate a YO-absorbing ^{15E}Pyo "ion pair" photoproduct with a re-aromatized chromophore. The ^{15E}Pyo photoproduct equilibrates with a R-absorbing ^{15E}Pr photoproduct, a process requiring Asp-205 and favored at low pH (as shown by this investigation). We envisage this process to entail a repositioning of the D-ring to interact with the Asp-205 carboxylate, likely in conjunction with rearrangement of the tongue region of the adjacent PHY domain seen in other phytochromes (30, 31, 48). This interconversion can be very fast (<seconds) or quite slow (>minute, as seen for *Np*TCCP) depending on TCCP species or variant. The ^{15E}Pyo/^{15E}Pr equilibrium also varies among TCCP family members and can be altered by site-directed mutations of conserved TCCP-signature residues in both GAF and PHY domains (as shown by this investigation). Both ^{15E}Pyo and ^{15E}Pr photoproduct states are photoactive because YO or R light can trigger regeneration of the ^{15E}Pvb dark-state. Residues in *To*TCCP, which likely interact with the chromophore are shown in parentheses. *B*, chromophore-contacting signature residues of *Sy*Cph1 and corresponding residues found in *To*TCCP. Shown is the chromophore-binding pocket of the *Sy*Cph1 GAF domain with PCB in the R-absorbing Pr state (PDB ID 2VEA) (28). The chromophore-binding pocket is drawn in surface representation (*light gray*). Labels refer to amino acid sequence numbers, and PCB is colored in *teal* and shown in stick form. Key chromophore-contacting residues are labeled with *black font* for *Sy*Cph1. *To*TCCP residues conserved with or diverged from those in Cph1 are labeled (in *brackets*) with *red* or *blue fonts*, respectively

residues located in GAF domains of phytobilin-based plant and cyanobacterial phytochromes or in the N-terminal PAS domains of BV-based bacterial, diatom and fungal phytochromes (8–14). More drastic blue shifts have been identified in cyanobacterial and eukaryotic algal phytochrome lineages, as well as in the distantly related GAF-only cyanobacteriochrome (CBCR) lineage; such shifts arise from additional Cys residues that form thioether linkages to their bilin chromophores (15–18).

Multiple dual-Cys CBCR lineages have been characterized to date (15, 16, 19–26). However, the tandem-Cys trichromatic phytochrome *Np*TP1 encoded by gene locus *NpunF1183* from *Nostoc punctiforme* ATCC 29133 is the only dual-Cys cyanobacterial phytochrome to have been investigated at the biochemical level (15). *Np*TP1's violet-blue (VB)-absorbing Pvb dark-state reflects a thioether linkage to the C10 methine bridge of its bilin prosthetic group that splits the tetrapyrrole π-conjugated system into two dipyrrole chromophores (15). *Np*TP1's forward photocycle is initiated by V-light, which triggers 15*Z* to 15*E* photoisomerization of the C15 double bond and subsequent destabilization of the C10 thioether linkage. Thioether cleavage generates an orange (O) light-absorbing Po intermediate that incompletely matures into an R-absorbing Pr photoproduct over a period of minutes. The reverse photocycle involves light-triggered 15*E* to 15*Z* isomerization followed by reformation of the C10 thioether lineage that regenerates the Pv dark-state (Fig. 1*A*).

The number of Tandem-Cysteine Cyanobacterial Phytochrome (TCCP) candidates has increased considerably because of the initial discovery of *Np*TP1, which we herein rename *Np*TCCP. TCCPs can be recognized by a conserved "second" Cys residue immediately adjacent to the "canonical" Cys site of phytobilin attachment in plant and cyanobacterial phytochrome lineages, and also share the photosensory core domain architectures of both phytobilin-binding Cph1/CphA and BV-binding BphP/CphB families of cyanobacterial phytochromes. Through biochemical and spectroscopic analysis of three phylogenetically diverged TCCPs identified from *de novo* draft genomes of *Tolypothrix* sp. PCC7910 (*To*TCCP), *Scytonema* sp. PCC10023 (*Sc*TCCP), and *Gloeocapsa* sp. PCC7513 (*Gl*TCCP), we resolve TCCPs as a monophyletic clade of VB-sensing cyanobacterial phytochromes that are distinct from the well-characterized R/FR cyanobacterial phytochromes. Our studies reveal unexpected spectral diversity in this dual-Cys cyanobacterial phytochrome family. From site-directed mutagenesis of *To*TCCP, pH-dependent spectroscopic measurements, and comparative analysis of tandem-Cys phytochrome sequences from eukaryotic algae (TCEPs), these investigations provide new insight into the structural basis of spectral tuning in the TCCP family, and the potential mechanistic roles of TCCP-signature residues in the novel photocycle of these V- to B-absorbing phytochromes.

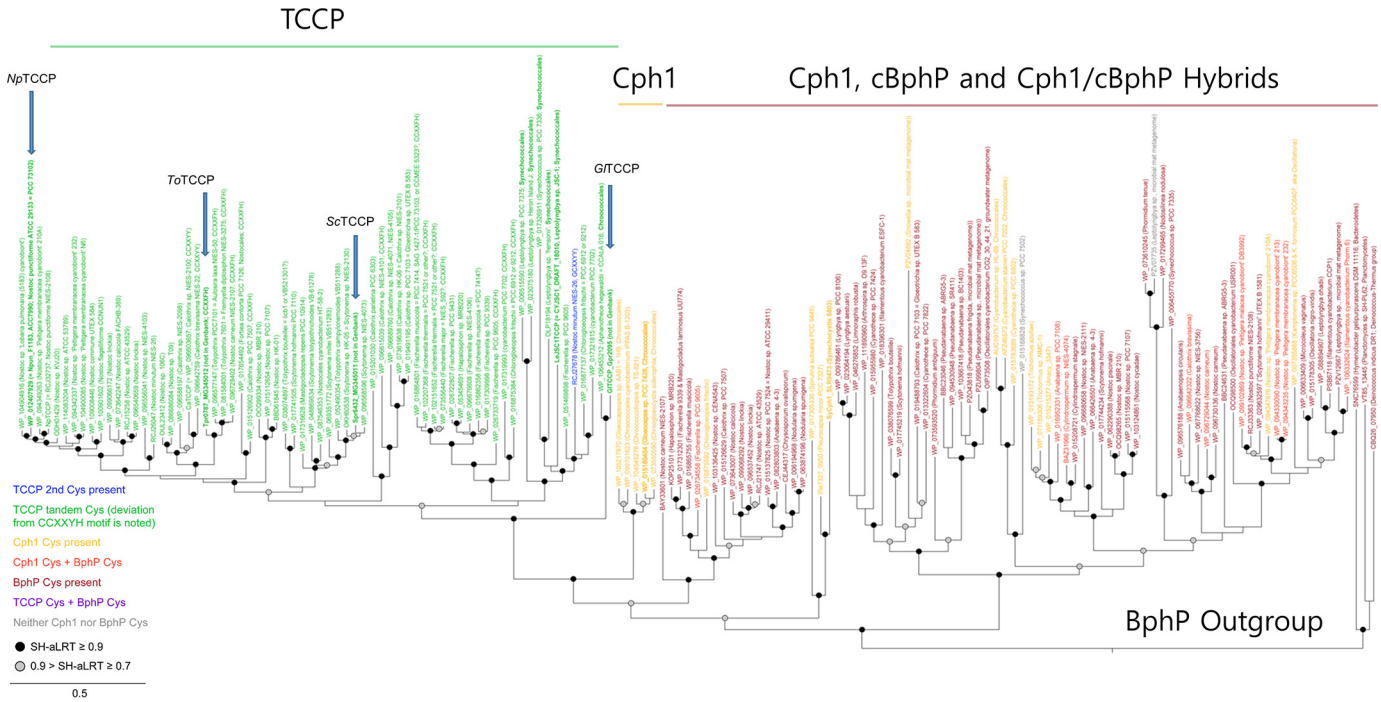

Figure 2. Phylogenetic analysis of photosensory core modules of TCCP, Cph1/CphA, and BphP/CphB family representatives supports a monophyletic TCCP lineage in cyanobacteria. The TCCP family consisting of *Np*TCCP (NpF1183) from *N. punctiforme* ATCC 29133 (15), orthologues *To*TCCP from *Tolypothrix* PCC7910 (Tpr0787), *Sc*TCCP from *Scytonema* PCC10023 (Spr6432), and *Gl*TCCP from *Gloeocapsa* PCC7513 (Gpr2095) studied here (indicated with *arrows*), comprise a monophyletic clade distinct from Cph1/CphA and BphP/CphB cyanobacterial phytochrome families. Noncyanobacterial BphPs are included as an outgroup. Detailed sequence names, accessions, and sequence alignments are included as in Data File S1.

Results

Multiple sequence alignments define a well-supported monophyletic TCCP lineage distinct from other cyanobacterial phytochrome families

A multiple sequence alignment of representative cyanobacterial TCCP, Cph1/CphA, and cBphP/CphB phytochrome families revealed the tandem-Cys and four other highly conserved residues within the PCB-binding GAF domain as defining hallmarks of the TCCP family (Fig. S1*A*, blue-colored residues). Leveraging a more comprehensive alignment (Data File S1), we resolved a monophyletic TCCP lineage, well-supported by bootstrap analysis and distinct from a polyphyletic group of Cph1/CphA and cBphP/CphB sequences (Fig. 2). Similar to *Sy*Cph1, the vast majority of TCCPs possess two component histidine kinase output domains (27) and occur in operons along with a CheY-like response regulator. The lone exception is the sensor from *Nostoc minutum* NIES26 that lacks the PHY domain as well as the canonical GAF-domain phytochrome Cys, *i.e.* Cys-259 in *Sy*Cph1 (*blue* labeled TCCP in Fig. 2). TCCPs retain most of the conserved chromophore-interacting GAF-domain residues found in Cph1 and BphP families (Fig. 1*B* and Fig. S1*A*). These include Arg-172, Tyr-176, Tyr-198, Tyr-203, Asp-207, Arg-222, Arg-254, Tyr-263, and His-290 (*Sy*Cph1 numbering), residues known to be critical to the structure and absorption properties of phytochromes. TCCP-signature residues in the GAF domain include Cys-258, His-262, Leu/Ile/Met-270, Val-272, and Ser-286 (*To*TCCP numbering, blue-colored residues in Fig. 1*B* and Fig. S1*A*). These replace residues highly conserved in Cph1 and BphP families, *i.e.* His-260, Leu-264, Ser-272, Thr-274, and Ala-288, respectively (*Sy*Cph1 numbering, shown in *black* in Fig. 1*B*). GAF domain residues with more variable substitutions in the TCCP family correspond to Val-254, Ala-256, and Gly-268 (*To*TCCP numbering, shown in *green* in Fig. S1*A*). The following studies were undertaken to address the hypothesis that these signature residues are important to TCCP spectral tuning.

TCCPs possess violet-blue–absorbing dark-states with spectrally diverse photoproducts

To determine chromophore binding specificity, we expressed recombinant PCMs of *To*TCCP, *ScTCCP*, and *Gl*TCCP in BV-, PCB-, or PΦB-producing *Escherichia coli* strains. The absorption spectra of the purified proteins were consistent with formation of covalent linkages to the bilin C10 methine bridge (Fig. 3, *A–F*). All three TCCPs possessed VB-absorbing (Pvb) dark-states with absorption maxima ranging from 401 to 435 nm (Table 1, Fig. 3, *A–C*, *blue*-colored spectra) similar to dual thioether adducts of *Np*TCCP (15). Zinc-dependent fluorescence imaging of SDS-PAGE gels (zinc blots) also indicated that the PCB and PΦB phytobilin chromophores of *To*TCCP, *ScTCCP*, and *Gl*TCCP remain covalently attached after denaturation (Fig. 3*G*). Like those of *Np*TCCP (15), BV adducts of *To*TCCP and *Sc*TCCP are unstable to denaturation, indicating that their A-ring thioether linkages (if present) in addition to their C10 linkages are chemically labile (Fig. 3*G*). By contrast, all three bilin adducts of *Gl*TCCP were more stable to denaturation and bilin incorporation was reduced compared with *To*TCCP and *Sc*TCCP. Based upon the difference spectra, the extent of photoconversion of the PCB adducts were greater than those of PΦB and BV adducts of all three TCCPs (Table 1,

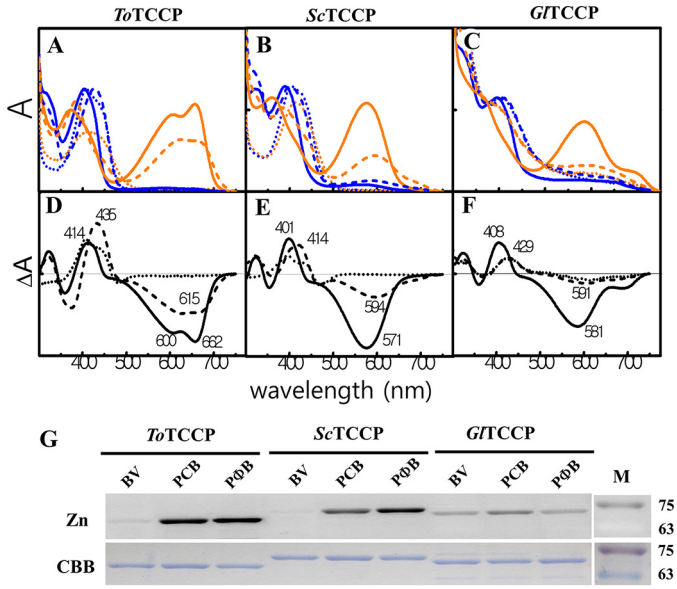

Figure 3. Spectral properties of bilin adducts of PCMs of recombinant *To*TCCP, *Sc*TCCP, and *Gl*TCCP proteins indicate differences in the ratio of two spectrally distinct 15*E* photoproducts in the TCCP family. Absorption spectra of PCMs of *To*TCCP (*A*), *Sc*TCCP (*B*), and *Gl*TCCP (*C*) incorporating PCB (*solid line*), BV (*dotted line*), or PΦB (*dashed line*) are shown in 15*Z* dark-states (*blue*) and 15*E* photoproducts (*orange*) in standard assay buffer at pH 8 (see "Experimental procedures"). Dark-minus-light difference spectra at pH 8 for native *To*TCCP (*D*), *Sc*TCCP (*E*), and *Gl*TCCP (*F*) were obtained from *panels A–C*, respectively. Zinc in-gel fluorescence and Coomassie Brilliant Blue (*CBB*) images of acid-denatured TCCPs (*G*) are shown. SDS-PAGE gels imaged by zinc-dependent in-gel fluorescence (*upper panel*) and after staining with CBB (*lower panel*) are shown. Molecular mass markers (M) in kDa are indicated on the *ordinate on the right side*.

Table 1

Absorption spectral parameters for TCCP sensors with different bilin chromophores

Recombinant photosensory core domain (PAS-GAF-PHY) constructs were purified after expression in *E. coli* cultures synthesizing BV, PCB, or PΦB (from Fig. 3 and Fig. S2) and desalted and concentrated in 50 mM Tris-HCl buffer, pH 8.

Protein	Bilin	λ_{max} [a] 15*Z*; 15*E*	SAR[b]	Y_c [c]	%ΔA[d]
*To*TCCP	BV	411; 424	0.22*	NA[e]	47.5 (0.287)
	PCB	414; 662	0.32	0.611	100 (0.604)
	PΦB	435; 615	0.25	0.502	91.4 (0.552)
*Sc*TCCP	BV	401; 401	0.26*	NA	27.1 (0.181)
	PCB	401; 571	0.23	0.385	100 (0.667)
	PΦB	414; 594	0.10	0.176	45.9 (0.306)
*Gl*TCCP	BV	426; 607	0.07*	NA	28.2 (0.072)
	PCB	408; 581	0.10	0.117	100 (0.256)
	PΦB	429; 598	0.02	0.024	44.5 (0.114)
*Np*TCCP	PCB	392; 598,670	0.22	NA	85.0

[a] Peak wavelengths are reported for the bilin transition of longest wavelength (S^1) as 15*Z* or 15*E*. Multiple values for the 15*E* state of *Np*TCCP reflect thermal evolution of the yellow-orange intermediate to a red-absorbing photoproduct (15).

[b] Specific absorbance ratio (SAR) values of acid-urea denatured proteins were calculated as the ratio of the peak absorbance of the bilin band and the protein band at 280 nm, serving as a relative measure of chromophore-binding efficiency. For BV adducts, SAR values indicated with asterisks correspond to native proteins due to instability of the presumed non-covalent adducts under acid denaturing conditions

[c] Chromophorylation yield (Y_c) was calculated as the ratio of bound chromophore to protein content (see "Experimental procedures" for details).

[d] Relative photoconversion efficiency of native BV- or PΦB- chromophorylated proteins (%ΔΔA) to respective PCB-chromophorylated proteins were provided. Photoconversion efficiency given in parentheses was determined by subtracting the 15*E* spectrum from the 15*Z* spectrum. Spectra were normalized to the blue band absorbance prior to the calculation. Values in parentheses are photoconversion efficiency.

[e] NA, not applicable.

Fig. 3, *D–F*). This supports the assumption that PCB is the preferred chromophore precursor of TCCPs because PΦB also is not produced by any known cyanobacteria and BV binding to the canonical Cys is rarely observed.

For PCB and PΦB adducts, we confirmed that light-induced photoisomerization had occurred by measurements of their photoactivity upon denaturation (Fig. S2, *A–C*). In the native state, none of three new TCCPs showed trichromatic cycles. The 15*E* photostate of the PCB adduct of *To*TCCP possessed both R-absorbing ^{15E}Pr (λ_{max} 662 nm) and O-absorbing ^{15E}Po (λ_{max} 600 nm) components (Fig. 3, *A* and *D*), similar to *Np*TCCP (15). However, formation of the R-absorbing 15*E* species for *To*TCCP was much faster than that for *Np*TCCP, which exhibits trichromatic photoproduct formation. Trichromatic behavior also was not seen for *Sc*TCCP or *Gl*TCCP. *Sc*TCCP yielded a single yellow-orange (YO) absorbing ^{15E}Pyo photoproduct with absorption maxima in the YO region, whereas *Gl*TCCP yielded a mixture of both ^{15E}Pyo and ^{15E}Pr photoproducts (Fig. 4, and Table 1). The observed photocycles for all three TCCPs are consistent with the model that 15*Z* to 15*E* photoisomerization of the VB-absorbing dark-state chromophores destabilizes the C10–Cys linkage initially to yield a significantly red-shifted ^{15E}Pyo photoproduct along with variable amounts of a ^{15E}Pr photoproduct, which sometimes appears over a long time (see conceptual model in Fig. 1*A*).

Cysteine mutagenesis reveals Cys-258 to be responsible for violet-blue absorption of TCCP dark-states, unmasking a latent G/R photocycle for ToTCCP

Because of its robust expression, we chose *To*TCCP for detailed mutagenesis studies to identify residues important for spectral tuning of its PCB adduct. Two variants of the canonical cysteine, *i.e.* C257A and C257S (*To*TCCP numbering), retained their VB-absorbing dark-states although neither was photoactive (Fig. 4, *A* and *B*). This result showed that Cys-257 was not needed for thioether linkage formation at the bilin C10 position. The C257A variant also was poorly chromophorylated, suggesting that the Cys-257 thioether linkage at $C3^1$ improves C10-linkage formation to Cys-258 similar to experiments performed for *Np*TCCP (15). Because C10 thioether linkages of bilins are chemically labile in solution, we examined whether stable linkages were retained in C257A and C257S variants following denaturation and zinc blot analysis. As expected, zinc blots for both Cys-257 variants were negative (Fig. S3). Taken together, these results indicate that Cys-258 is sufficient for C10 linkage formation and for retention of the VB absorption of *To*TCCP's dark-state.

We next examined *To*TCCP variants of the TCCP-signature cysteine, *i.e.* Cys-258 (*To*TCCP numbering). These included C258H, C258S, C258D, C258I, C258F, and C258Y, all of which yielded red-shifted dark-states (Fig. 4, *C–H*). As expected, C258H displayed R-absorbing 15*Z* dark-state similar to Cph1, which has a histidine residue at this position (Fig. 4*C*). By contrast, C258S, C258D, and C258I exhibited G-absorbing dark-states with variable amounts of a R-absorbing species, whereas C258F and C258Y dark-states displayed broad YO-absorbing envelopes (Fig. 4; Table 2). Of these Cys variants, C258S, C258D, and C258I were photoactive and all exhibited atypical

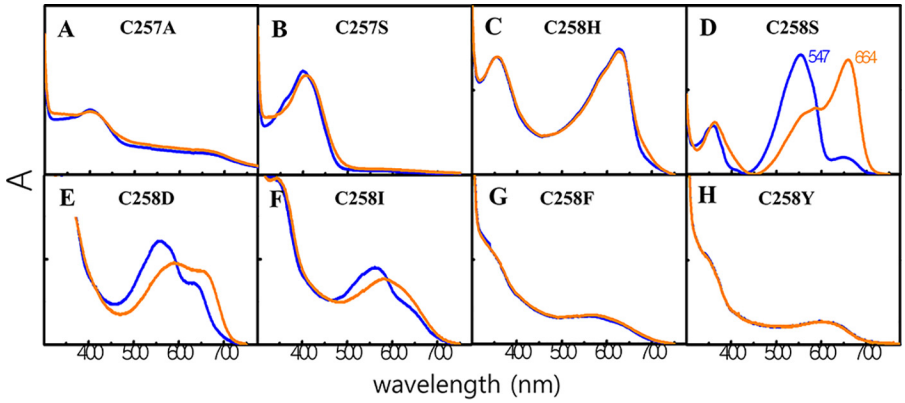

Figure 4. Absorption spectra of Cys variants of *To*TCCP indicates an essential role for the TCCP-signature cysteine in forming the B-absorbing 15*Z* dark-state. Absorption spectra of PCMs of *To*TCCP, canonical Cys variants, C257A (*A*) and C257S (*B*), and TCCP-signature cysteine variants, C258H (*C*), C258S (*D*), C258D (*E*), C258I (*F*), C258F (*G*), and C258Y (*H*), at pH 8 incorporating PCB are shown for 15*Z* dark-states (*blue*) and 15*E* photoproducts (*orange*). The loss of the canonical Cys in C257A/C257S variants yields a B-absorbing 15*Z* species that affords a stable B-absorbing 15*E* state because of the apparent stability of the C10 linkage. The loss of the TCCP-signature Cys (C258H/C258S/C258D/C258I/C258F/C258Y) yields red-absorbing variants in both 15*Z* and 15*E* states due to the loss of the C10 thioether linkage.

Table 2

Spectral properties of PCB-adducts of *To*TCCP wild type and variants

Recombinant photosensory core domains (PAS-GAF-PHY) of *To*TCCP were purified after expression in *E. coli* cultures synthesizing PCB (from Figs. 4 and 5) and desalted and concentrated in 50 mM Tris-HCl buffer, pH 8. Label abbreviations are defined in Table I.

Protein	λ_{max}	SAR[a]	%ΔΔA	Reverse photocycle	Remarks
Wildtype	402; 662	0.191	100	Y	
Cys variants					
C257A	402; 402	0.06	NA[b]	N	Canonical 1st Cys
C257S	398; 402	0.107	NA	N	
C258H	627; 627	0.114	NA	N	TCCP specific axial Cys
C258S	547; 664	0.318	100	Y	
C258D	552; 672	0.027	85.4	Y	
C258I	566; 610	0.021	67.7	Y	
C258F	545; 545	0.011	NA	N	
C258Y	580; 580	0.010	NA	N	
C287S	403; 663	0.159	94.5	Y	Cph conserved Cys
C303S	403; 663	0.179	86.9	Y	Cph conserved Cys
Other variants					
H262L	427; 665	0.121	98.1	Y	TCCP signature
H262Y	403; 662	0.146	80.4	Y	
L270S	398; 662	0.231	139.9	Y	
V272T	402; 598, 604	0.454	22.9, 35.9	Y	
V272S	408; 578	0.235	77.6	Y	TCCP signature
S286A	396; 598, 662	0.168	57.3, 84.9	Y	TCCP signature
V254F	408; 660	0.122	98.1	Y	Variant in *Np*TCCP
A256W	407; 658	0.097	75.7	Y	Variant in *Np*TCCP
F261Y	404; 602	0.045	70.4	Y	Variant in *To*TCCP
F261W	405; 602, 662	0.109	43.6, 85.4	Y	
G268K	411; 659	0.053	101.6	Y	Variant in *Np*TCCP
D205N	405; 597	0.088	45.4	Y	
Y174F	403, 578	1.04	52	Y	
Y174H	405, 565	0.81	50.6	Y	
H288A	382, 583	0.64	21.9	Y	
Y201F	403, 655	0.84	75.7	Y	

[a] Specific absorbance ratio (SAR), a measure of chromophorylation, is the ratio of absorbances at the longest wavelength absorption maximum of the dark state and at 280 nm.
[b] NA, not applicable.

G/R photocycles. By comparison, C258H, C258F, and C258Y were photoinactive. All Cys-258 variants also retained stable covalent linkages as shown by zinc blotting, although the reduced zinc blot signals for C258I, C258D, C257Y, and C258F are likely due to poor PCB binding (Fig. S3). These observations indicate that Cys-258 plays an essential role in spectral tuning of the VB-absorbing dark-state of *To*TCCP.

In view of the robust G/R photocycle observed for the C258S variant of *To*TCCP (Fig. 4*D*), we constructed the corresponding Cys-to-Ser variants for *Gl*TCCP (C249S) and *Sc*TCCP (C257S). Unlike the C258S variant of *To*TCCP, *Gl*TCCP (C249S) and *Sc*TCCP (C257S) variants exhibited mostly R-absorbing (λ_{max} 645 nm) or mostly green (G)-absorbing (λ_{max} 530 nm) dark-state mixtures, respectively, that were strongly bleached upon light treatment (Fig. S4, *A*, *B*, *E*, and *F* and Table 2). These results show that the spectral consequences of substitution of the TCCP-signature cysteine with serine are species dependent and difficult to predict.

Highly conserved in all cyanobacterial phytochrome families (Fig. S1*A*), Cys-287 and Cys-303 in *To*TCCP are located in good positions to form a disulfide linkage (28). For this reason, we also constructed C287S and C303S variants to test the impor-

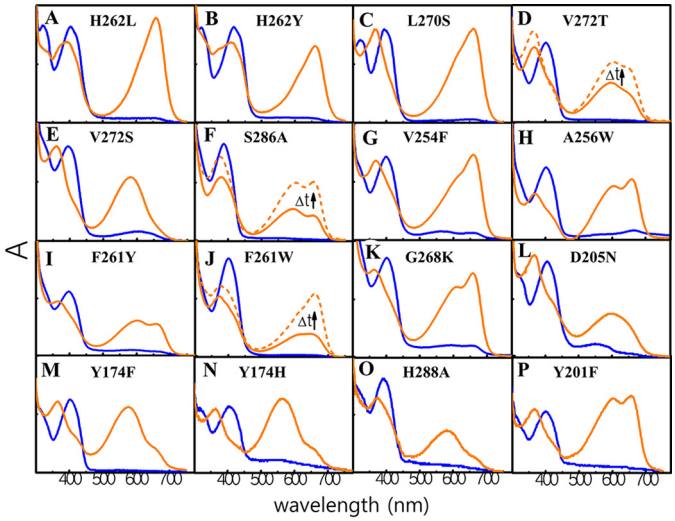

Figure 5. Absorption spectra of *To*TCCP variants in TCCP family-specific, *To*TCCP-specific, and TCCP-family variable residues reveal selective roles in spectral tuning in the TCCP family. 15*Z* dark-states are shown in *blue*, 15*E* photoproduct states shown in *orange* before and after dark maturation (*solid* and *dashed*, respectively). Zinc in-gel fluorescence data for all mutants are shown in Fig. S3.

tance of these cysteine residues in the *To*TCCP photocycle. The spectra and photocycles of these variants were almost indistinguishable for those of the WT parents (compare Fig. S4, *C*, *D*, *G*, and *H* with Fig. 3, *A* and *D*). Because natural variation is seen at both cysteines in all cyanobacterial phytochrome lineages, it appears that disulfide bond formation between this conserved Cys pair is not necessary for native TCCP photocycles.

Mutagenesis of conserved TCCP species-specific residues reveals potential roles in photoproduct spectral tuning

To identify residues affecting photoproduct tuning in the TCCP family, we exchanged representative TCCP-signature residues in *To*TCCP with those found in Cph1 and BphP families. Residues initially targeted for mutagenesis included two with hydrophilic side chains, *i.e.* His-262 and Ser-286 (*To*TCCP numbering), and two with hydrophobic side chains, *i.e.* Leu-270 and Val-272 (*To*TCCP numbering), which correspond to *Sy*Cph1 residues Leu-264 located in α8, Ala-288 located in β11, and Ser-272 and Thr-274 located in β10, respectively (see Fig. 1*B* and Fig. S1). We generated five *To*TCCP variants by replacement of these four residues with those found in *Sy*Cph1 and additional variants of His-262 and Val-272 that occurs infrequently in the TCCP family. The absorption spectra of the dark-states of all variants were similar to those of the WT (Fig. 5, *A–E*, *blue spectra*; Table 2). By contrast, the photoproduct spectra of these variants all differed from that of WT *To*TCCP (Fig. 5, *A–E*, also see Fig. S5, *A–E* for difference spectra). Instead of the dual-peaked spectrum of the WT *To*TCCP, photoproducts of H262L, H262Y, and L270S variants exhibited R-absorbing peaks lacking the YO-absorbing shoulder. Interestingly, the photoproduct spectra of V272T and V272S variants were not identical to each other, with the former exhibiting delayed formation of a photoproduct mixture similar to *Np*TCCP and a single Y-absorbing peak being observed for the latter. The S286A variant also exhibited delayed formation of a photoproduct mixture similar to *Np*TCCP. These observations indicate that the four TCCP-conserved residues are not important for the dark-state spectra, but all participate in spectral tuning of the *To*TCCP photoproduct. Moreover, none of the variants examined yielded a FR-absorbing 15*E*-photoproduct seen in the Cph1 family. It is therefore likely that multiple changes in these conserved residues are required to further red shift TCCP photoproducts into the far-red.

*To*TCCP residues not well-conserved in the TCCP family were also investigated, including Val-254, Ala-256, Phe-261, and Gly-268 (Fig. S1*A*, highlighted in *green*). We hypothesized that the trichromatic photocycle might be restored by substituting these residues with those found in the trichromatic *Np*TCCP. Among the variants tested (Fig. 5, *G–K*), only the F261W variant exhibited delayed formation of a mostly R-absorbing photoproduct similar to *Np*TCCP, although V254F also yielded a R-absorbing photoproduct. By contrast, the photoproduct spectra of A256W, F261Y, and G268K were quite similar to WT *To*TCCP. These results highlight supporting roles for Val-254 and Phe-261 in TCCP photoproduct spectral tuning.

We also examined *To*TCCP variants in strongly conserved residues in the extended phytochrome superfamily. These included D205N, Y174H/Y174F, H288A, and Y201F, to target chromophore contacting residues known to play important roles in spectral tuning in Cph1 and BphP families. Asp-205 corresponds to *Sy*Cph1 residue Asp-207, an invariant residue that has been proposed to function as a counterion for the cationic protonated bilin chromophore (28). D205N yielded an O-absorbing photoproduct with very little R-absorbing photoproduct (Fig. 5*L*). The photoproducts of both variants of Tyr-174, *i.e.* Y174F and Y174H, as well as the variant H288A were also enriched in the YO-absorbing species (Fig. 5, *M–O*). Although the inclusion of imidazole in the assay buffer might influence the spectra of His variants, at 250 μM it is unlikely to have a significant differential effect on TCCP variants reported here. Only the photoproduct of the Y201F variant was quite similar with WT *To*TCCP (Fig. 5*P*), underlying the universal importance of the nearly invariant Asp-205, Tyr-174, and His-290 residues in photoproduct tuning in all phytochrome lineages.

Spectroscopic titration of ToTCCP and its singly-linked C258S variant reveals pH-dependent equilibria between R-absorbing protonated and G-absorbing deprotonated states

To test whether the varying ratio of YO- and R-absorbing photoproducts is due to differences in ionization states of the chromophore and/or nearby amino acid residues, we undertook experiments to test the effect of pH on the *To*TCCP photoproduct spectrum, an approach was used previously to examine the pH-dependence of both dark and photoproduct states of the G/R CBCR RcaE (29) and the B/O CBCR Oscil6304_2705 (26). As expected for a neutral doubly-linked chromophore (Fig. 1*A*), we first confirmed that the spectrum of 15*Z* dark-state of *To*TCCP was unaffected by changes in buffer pH (Fig. 6*A*). By contrast, the 15*E* photoproduct state spectrum of *To*TCCP was strongly pH-dependent, supporting the assignment of the YO-absorbing (579 nm) and R-absorbing (663 nm) species to deprotonated and protonated photoproducts, re-

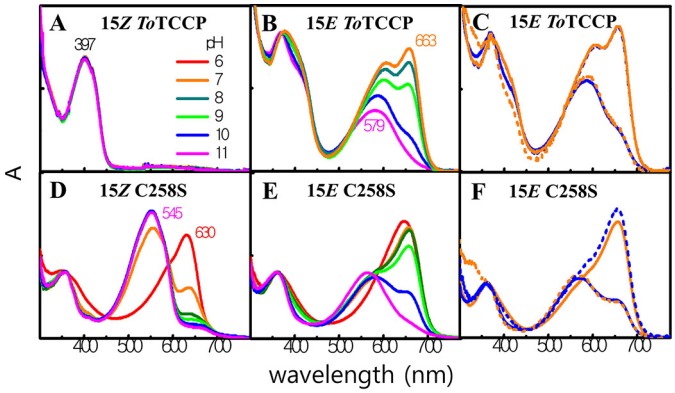

Figure 6. Spectroscopic pH titrations of *To*TCCP and its singly-linked C258S variant reveals pH-dependent equilibria between G- and R-absorbing species. *To*TCCP WT and C258S variant in 15*Z* dark and 15*E* lit states at pH 8 were adjusted to different pH values (see "Experimental procedures" for details). All spectra are normalized to the same concentration in *panels A*, *B*, *D*, and *E*. In *panels C* and *F*, the 15*E* photoproduct at pH 7 and 10 (*solid curves*, *blue* pH 10, and *orange* pH 7) were adjusted to pH 7 or 10 (*dashed curves*, *blue* pH 7 and *orange* pH 10). Normalized spectra shown are superimposed.

spectively (Fig. 6*B*). Based on these studies, we estimated an apparent pK_a of 9.5 for the titratable group(s) responsible (Fig. S6*A*). pH shift measurements were also performed as a control to test whether these spectral changes were reversible after cycling the pH from pH 10 to 7, and vice versa. These experiments indicated that the spectra of the fully deprotonated and fully protonated photoproduct species were identical before and after each pH shift (Fig. 6*C*), thereby establishing that *To*TCCP is not irreversibly denatured in this pH range.

pH titrations of both photostates of the C258S variant of *To*TCCP were next examined. The photocycle of this variant (Fig. 4*D*) is very similar to that of the G/R CBCR RcaE whose G-absorbing 15*Z* dark-state chromophore is deprotonated and its R-absorbing 15*E* photoproduct chromophore is protonated (29). Like RcaE, both 15*Z* and 15*E* states of the C258S variant were pH-sensitive. The G-absorbing 15*Z* dark-state could be converted to a R-absorbing species with a peak at 635 nm and the shorter wavelength-absorbing shoulder of the 15*E* photoproduct could be eliminated by lowering the pH to 6 (Fig. 6*D*). Based on this titration experiment, an apparent pK_a of 6.6 was estimated for the titratable group(s) responsible for the spectral shift of the 15*Z* dark-state (Fig. S6*B*). The presence of clear isosbestic points also corroborates a two-species model. We next performed a pH titration experiment with the 15*E* photoproduct of the C258S variant (Fig. 6*E*). Similar to WT *To*TCCP, the pH-dependent equilibrium between R- and G-absorbing species revealed a titratable group(s) with an apparent pK_a of 9.7 (Fig. S6*C*). pH-shift spectroscopic measurements also indicated that titrations of the C258S variant were reversible in both directions (Fig. 6*F*) showing that C258S was not denatured in the pH 7–10 range.

pH dependence of other ToTCCP variants reveals complex interplay of signature GAF-domain residues in photoproduct tuning

To explore the influence of TCCP-signature residues on spectral tuning of the 15*E*-photoproduct of *To*TCCP, we examined the pH dependence of the eight previously described *To*TCCP variants, D205N, V254F, F261G/W, H262L, L270S, V272T, and S286A. In this experiment, each variant was examined spectrophotometrically at pH 6, 8, and 11. All variants bound PCB and exhibited YO-absorbing spectra at pH 11 (Fig. 7). With the exception of D205N, we observed an increase in the R region as the pH was lowered to pH 6 for the photoproduct 15*E* states of all variants (Fig. 7*A*). Of these variants, only V272T and S286A retained significant YO absorption at pH 6 (Fig. 7, *G* and *H*). Surprisingly, the YO peak intensity of V272T increased as the pH was lowered from 11 to 6. A similar spectral change was seen for S286A except that the maximum amount of red-absorbing species was fully formed at pH 8 and remained unchanged as the pH was further lowered to 6. These results suggest that a second YO species with a larger absorption coefficient was produced as the pH was lowered to 8 for the V272S and S286A variants. A similar phenomenon was seen for the V254F and F261W variants, although both second YO and R peaks increased and then partially disappeared as the pH was lowered to 8 and then to 6 (Fig. 7, *B* and *D*). For these experiments, photoproduct heterogeneity was evident by the lack of clear isosbestic points in pH titrations of V254F, F261W, and V272S variants (Fig. 7, *B*, *D*, and *G*). By contrast with the appearance of the second YO species, F261G, H262L, and L270S variants exhibited a stepwise direct conversion to an R-absorbing species as the pH was lowered from 11 to 6 (Fig. 7, *C*, *E*, and *F*). Clear isosbestic points were seen in F261G and H262L spectrophotometric titrations indicating the presence of two species in pH-dependent equilibrium. As controls, seven of the eight variants except the Y-absorbing D205N variant retained photoreversibility upon forward or reverse cycling from pH 7 to 10 buffer (Fig. S7). D205N yielded a mixture of G- and V-absorbing species at pH 10 upon photocycling to/from each photostate. This suggests that the D205N mutant is irreversibly denatured by high pH.

PHY domain variants reveal participation of the PHY domain in the conversion between the YO- and R-absorbing photoproducts

In single-Cys phytochromes such as Cph1, BphP, and *At*PHYB, PHY domain motifs WGG, PR*X*SF, and Hb*X*E have been shown to stabilize the 15*E* Pfr photoproduct state (30, 31). For example, variants in WGG (G564E) and PR*X*SF (R582A) motifs of phyB inhibited thermal "dark" reversion of Pfr (31). Because these PHY domain motifs are also conserved in the TCCP family (Fig. S1*B*), we constructed the A451G, R471A, R471K, K472F, and E479A variants of *To*TCCP to target their role in stabilizing one or both of the photoproduct states (Fig. S8). R471A and R471K variants yielded only the ^{15E}Pyo photoproduct. All other PHY domain variants afforded final product mixtures with spectra very similar to that of the WT, although product maturation was considerably delayed in A451G and E479A variants. These results suggest that the photoproduct red shift is influenced by interactions with the PHY domain, consistent with studies on the formation of the Pfr state in prototypical plant and cyanobacterial phytochromes that lack the PHY domain (32).

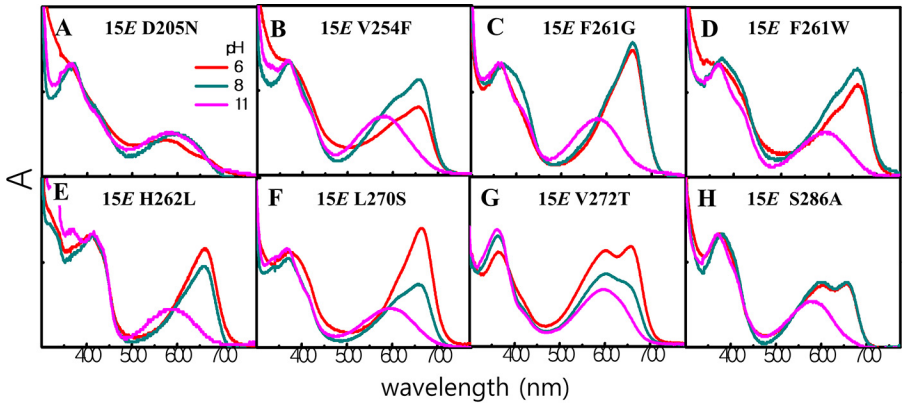

Figure 7. pH dependence of selected variants of *To*TCCP indicates that the 15*E* photoproduct comprises a mixture of spectrally distinct YO-absorbing "deprotonated" and R-absorbing "protonated" states. *To*TCCP variants after conversion to their 15*E* photoproduct states were adjusted to different pH values (see "Experimental procedures" for details). Spectra for each indicated variant are colored by pH as follows: pH 6 (*red*), pH 8 (*green*), and pH 11 (*fushia*).

Discussion

Our studies resolve a phylogenetically distinct clade of PCB-binding TCCP lineage of two-Cys cyanobacterial phytochromes, which are mostly restricted to members of the more recently evolved subsection IV and V clades of filamentous, nitrogen-fixing cyanobacteria (Fig. 2). Evolution of this group coincided with increasing atmospheric oxygen accumulation during the Great Oxidation Event (33). Filamentous growth observed in multicellular cyanobacteria would be advantageous in improving cell motility as well as metabolic fitness compared with unicellular cyanobacteria (33, 34). TCCPs sense V-to-B light and yield photoproducts that absorb in the YO and/or R spectral regions. Both long-wavelength–absorbing photoproducts appear after photoisomerization of the dual-linked, dark-state chromophore, a process that destabilizes the C10-thioether linkage (Fig. 1*A*). Our studies show that the equilibrium between YO- and R-absorbing photoproducts is pH-dependent. This suggests that TCCP sensors may be able to integrate light quality and cellular pH, both of which vary throughout the diurnal light-dark cycle and from light fluctuations in the natural environment due to changes in depth or shading by neighbors. The ability to sense and utilize B-, G-, and YO-light for photosynthesis is invaluable to cyanobacterial species, which live at depth where R and FR light are strongly attenuated in water. This selective pressure likely was one of the factors contributing to the evolution of TCCPs as well as the more spectrally diverse CBCR family.

Aside from the tandem cysteines, TCCP-signature residues play a minimal role in spectral tuning of the 15Z dark-state

Our cysteine mutagenesis studies establish that formation of the C10 thioether linkage does not require the canonical cysteine to generate the VB-absorbing 15*Z* dark-state (Fig. 4, *A* and *B*). However, the canonical cysteine is needed for photoactivity because the C257A and C257S variants are photochemically inactive. This implies a critical role for the canonical Cys linkage, *e.g.* for proper positioning of the bilin chromophore in the protein pocket. All variants of the TCCP-signature cysteine that bound bilin exhibited significantly red-shifted dark-states with absorption maxima that varied from green to orange. This corroborates the observations of previous studies that show the TCCP-signature cysteine to be essential for dark-state tuning (15). Several of these variants, *i.e.* C258S, C258D, and C258I, yielded G-absorbing dark-states similar to those of G/R CBCRs such as *Fd*RcaE (Fig. 4, *D–F*). Indeed, spectrophotometric titrations on the C258S variant indicate that the G- and YO-species are interconvertible via a pH-dependent process with an apparent pK_a of 6.6 (Fig. 6*D* and Fig. S6*B*), a result similar to the dark-state of the G/R CBCR *Fd*RcaE (29). However, the protonated dark-state species of *Fd*RcaE maximally absorbs in the red region, not in the YO region. These results support the interpretation that the G-absorbing chromophore of the C258S dark-state is deprotonated, whereas the protonated YO-absorbing 15*Z* chromophore adopts a more distorted out-of-plane geometry that blue-shifts its absorption maximum. The C258H variant, which restores the conserved "axial" histidine residue found in all R/FR phytochromes, also absorbs mostly in the yellow-orange region. This suggests that the C258H dark-state chromophore is fully protonated at pH 7.5, similar to phytochromes albeit with a more distorted chromophore that yields a blue-shifted absorption maximum.

Mutagenesis of TCCP-signature residues revealed little influence on 15*Z* dark-state tuning of *To*TCCP. With the exception of variants in the tandem cysteine pair, none of signature residue variants, *i.e.* His-262, Leu-270, Val-272, and Ser-286 (*To*TCCP numbering; Fig. 1*B*) abolished second thioether linkage formation nor appreciably altered the VB absorption of their 15*Z* dark-states (Fig. 5*A*). Because both 15*Z-syn* and 15*Z-anti* configurations at C15 are compatible with a VB-absorbing dark-state, it is possible that one or more of these variants could have affected the C15 configuration while not affecting dark-state absorption. Moreover, the pH has little or no effect on the 15*Z* dark-state absorption of TCCPs, with the exception of *Gl*TCCP whose second thioether linkage is sensitive to extreme pH values (Fig. 6 and Fig. S9). This is reasonable because the double linkage splits the PCB chromophore into two uncharged dipyrroles neither of which can donate or accept a proton in the pH 6–11 range used in this study (35).

With the exception of Ser-286, TCCP-signature residues are predicted to be located on the α-facial side of the chromophore (Fig. 1*B*, residues in *blue*). This includes the TCCP-signature cysteine that constrains the thioether linkage to Cys-258 to be α-facial, which contrasts with the β-facial C10 linkage found

in the dual-cysteine CBCR TePixJ and related CBCRs (16, 36). The dual α-facial linkages constrain the A-B ring system to be closely appressed to the α8 helix and likely prevent binding of the α-facial pyrrole water found in canonical phytochromes. The α-facial C10 linkage would also require the C-D ring system to tilt toward the β-face of the chromophore pocket. This orientation would preclude H-bonding between the D-ring carbonyl and the imidazole side chain of His-288, a highly conserved residue known to stabilize the 15*Z-anti* configuration of Pr chromophores in prototypical phytochromes (28, 37). The lack of this interaction in the doubly linked species may affect the equilibrium between the C15-*syn* and C15-*anti* conformations for the 15*Z* dark-state. The exchange of the polar residues in the β10 strand in Cph1, *i.e.* Ser-272 and Thr-274, with nonpolar residues in TCCPs, *i.e.* Leu-270 and Val-272 in *To*TCCP, also ensures that polar interactions with the bilin propionates do not occur. The relatively nonpolar pocket of TCCPs compared with Cph1/BphP families as well as the neutral charge of the doubly linked chromophore may also influence the ionization state of one or both propionic acid side chains of the 15*Z* dark-state chromophore. For this reason, we hypothesize that the B-ring propionic acid is protonated and neutral in the 15*Z* dark-state as depicted in Fig. 1*A*. Based on modeling of the *To*TCCP dark-state using *Dr*BphP and *Sy*Cph1 dark-state structures as templates (PDB IDs 2O9B and 2VEA), we propose that the β-facial serine 286 is located in a good position to stabilize the 15*Z-anti* configuration of the dark-state chromophore via H-bonding with the D-ring carbonyl (see Fig. 1*B* and Fig. S1*A*). However, this hypothesis remains to be tested. Because the B-absorbing dark-state absorption is not expected to change much by the C15 *syn*-to-*anti* conversion, the 15*Z-syn* configuration of the *To*TCCP dark-state at present remains a formal possibility.

pH plays a critical role in the ^{15E}Pyo:^{15E}Pr photoproduct equilibrium

By contrast with dual-linked dark-states, the TCCP photoproduct equilibrium is strongly affected by pH. For nearly all WT and variant TCCPs studied, we observed a mixture of YO- and R-absorbing photoproducts whose ratio is affected by both pH and signature residue substitutions. Primarily based on evidence that the D205N variant of *To*TCCP adopts an O-only photoproduct state at all pH values (Fig. 7*A*), we initially favored assignment of the O- and R-absorbing photoproducts to species with deprotonated-neutral and protonated-cationic π systems, respectively. The G/R photocycle of the C258S mutant also is consistent with the hypothesis that the initial 15*E*-photoproduct of WT *To*TCCP would possess a neutral deprotonated bilin chromophore and a neutral protonated Cys-258 sulfhydryl side chain. However, such a neutral state would equilibrate with a zwitterionic ^{15E}Pyo state with a protonated cationic 15*E-anti* bilin system and an anionic sulfhydryl on Cys-258 as shown in Fig. 1*A*. We also hypothesize that the His-262 side chain is located in a good position to stabilize this sulfhydryl anion upon transfer of a proton from the B-ring propionic acid to generate an imidazolium cation that bridges the propionate and sulfhydryl anions as depicted in lit State 1 in Fig. 1*A*.

Because acid-denatured biliproteins with 15*E* bilin chromophores absorb YO rather than G light (29, 38, 39), we favor the interpretation that the ^{15E}Pyo photoproduct possesses a protonated bilin chromophore at pH 8, also consistent with the zwitterionic Lit State 1 structure. Although low pH favors conversion of Lit State 1 to Lit State 2 by protonating the Cys-258 sulfhydryl, which would disrupt its ion-pair interaction with the protonated chromophore, this interconversion likely involves more substantive changes in the interactions between the GAF and PHY domains. We therefore hypothesize that the observed ratio of ^{15E}Pyo to ^{15E}Pr photoproducts represents the equilibrium between two protonated chromophore states whose energetics reflect distinct networks of pH-dependent H-bonding, ion-pair, and steric interactions. Because our spectral titration studies reveal an "apparent" pK_a of 9.5 for the conversion between the two 15*E* photoproducts of WT *To*TCCP (Fig. S6*C*), we tentatively assign this equilibrium to the ionization of the Cys-258 sulfhydryl group.

We envisage the ^{15E}Pyo and ^{15E}Pr conversion to be accompanied by significant changes in chromophore-protein interactions upon sulfhydryl protonation, such as counterion exchange for both propionate ion pairs, disruption of the Asp-205–Arg-471 ion pair between GAF and PHY domains, restructuring of the secondary structure of the tongue motif as well as formation of new H-bonding and ion pair interactions between protein residues and the bilin chromophore (30, 42, 43). Hence, the pK_a estimate from titration experiments likely entails contributions from multiple weak acid species that affect the kinetics and thermodynamics of this interconversion. Moreover, TCCP photoactivation also is expected to influence intersubunit interactions in the full-length homodimer and those of the truncated TCCP photosensory modules studied here that appear to be dimers by native gel electrophoresis and steric exclusion chromatography. Thus, the level of chromophorylation might play a critical role in stabilizing the fully activated state of the TCCPs. Because these intersubunit interactions are likely to be pH-dependent, the variable ^{15E}Pyo to ^{15E}Pr ratios for the four TCCPs examined here and previously (15) also may be influenced by different ratios of partially and fully chromophorylated dimers. Indeed, recombinant TCCPs from *E. coli* are poorly chromophorylated. Hence, it is conceivable that the variable "equilibria" between the two photoproduct states of TCCPs arises from different ratios of partially and fully chromophorylated species that affects the relative energetics of the two photoproduct proteins.

It is well-established that both 15*E* and 15*Z* chromophores of Cph1 are inherently heterogeneous (44–47). Such heterogeneity might be due to *15-syn versus 15-anti* chromophore configurations, α- *versus* β-facial dispositions of the D-ring, A-ring out-of-plane twisting, alternative protein-chromophore H-bonding networks, and/or relaxed *versus* trapped twist conformations of the D-ring (40, 41), any of which are formal possibilities for the pH-dependence of the ^{15E}Pyo:^{15E}Pr photoproduct ratio. Because the chromophore pocket of dark states of phytochromes, and those of TCCPs by analogy, are relatively solvent inaccessible, proton transfer rates from bulk solvent to the chromophore could be quite impaired, requiring re-orientation of proton donor and proton acceptor groups, including

water, that may be strongly constrained within the chromophore-binding pocket and requiring disruption and reformation of strong secondary interactions like those observed following bacteriophytochrome *Dr*BphP photoactivation that have a formidable energetic barrier to accomplish (48).

TCCP-signature residues strongly influence the ^{15E}Pyo:^{15E}Pr photoproduct equilibrium

Our mutagenesis studies corroborates the interpretation that the protonation state of the TCCP-signature cysteine plays a dominant role in the ^{15E}Pyo:^{15E}Pr equilibration process. Compared with WT at pH 8, the C258S variant exhibits an enhanced yield of the R-absorbing ^{15E}Pr photoproduct (Fig. 4*D*). Isosteric with Cys, Ser cannot be deprotonated to stabilize a YO-absorbing ion pair with the protonated bilin system, thereby favoring the ^{15E}Pr photoproduct. By contrast, the C258D variant favors the ^{15E}Pyo photoproduct (Fig. 4*E*), which could be rationalized by its low pK_a and difficulty to protonate *in situ*. However, it is also possible that the aspartate variant could interact with nearby cationic residues, *e.g.* His-262, Arg-220, or Arg-254, to inhibit the interconversion to the Lit State 2. Substitution of Cys-258 with amino acids with larger side chains, *i.e.* C258L, C258L, and C258Y, affected both the yield of chromophore attachment and the photochemical activity (Fig. 4, *F–H*). This suggests that these variants alter the positioning of the bilin chromophore possibly to minimize unfavorable steric interactions. In view of the altered photoproduct equilibrium of the Y174F and Y174H variants, it is also possible that Tyr-174 anion formation can destabilize the R-absorbing species at high pH possibly by disruption of an H-bond between the ionized C-ring propionate observed in the ^{15E}Pfr form of bacteriophytochromes (42). However, this interpretation cannot be responsible for other mutations that favor the ^{15E}Pyo species, *i.e.* D200N and H288A. Until the crystal structures of the ^{15E}Pyo and ^{15E}Pr photoproducts are resolved, we favor the interpretation that the Cys-258 thiol ionization is the primary determinant for regulating the ratio between the two photoproduct states (Fig. 1*A*).

In addition to the C258S variant, variants H262L, H262Y, L270S, V254F, and F261W all exhibited increased amounts of the ^{15E}Pr photoproduct (Fig. 5, *A–C*, *G*, and *J*). We envisage that these variants destabilize the ^{15E}Pyo photoproduct possibly by increased steric clashes or by gain/loss of H-bonding interactions with the bilin propionate side chains. Indeed, most of these variants restore residues found in phytochromes that stabilize the ^{15E}Pfr photoproduct state. We also observed that some of the *To*TCCP variants slow down the conversion between the two states without altering the final equilibrium, *i.e.* V272T, S286A, and F261W (Fig. 5, *D*, *E*, and *J*), similar to the photocycle of *Np*TCCP (15). We attribute the effect of these variants to an increase in the energetic barrier between the ^{15E}Pyo to ^{15E}Pr conversion that likely alters the rearrangement dynamics of the PHY tongue region following photoisomerization seen in cyanobacterial, plant, and (bacterio)phytochromes (30, 31, 48). Moreover, R471A or R471K variants favor the ^{15E}Pyo photoproduct, indicating that this Asp-205– contacting residue found in the PHY domain also plays an important role in photoproduct tuning in *To*TCCP. Although none of the other variants in PHY domain, *i.e.* A451G, E479A, and K472F, appreciably influenced the photoproduct ratio, a minor role of these residues in *To*TCCP photoproduct tuning.

Tandem-Cys phytochromes have also evolved in the eukaryotic algae

Although short-wavelength–absorbing streptophyte alga and land plant phytochromes so far have not been identified, B-, G-, Y- and O-sensing phytochromes have diversified in eukaryotic algae (17). Evidence for independent evolution of tandem-cysteine phytochromes has been reported in glaucophyte alga, the most ancient eukaryotic algal lineage (17). The present studies suggest that a small number of amino acid substitutions within the GAF domain may be sufficient to transform a Cph1 (or BphP) into a fully photoswitchable TCCP variant. These substitutions correspond to four signature positions, His-262, Leu-270, Val-274, and Ser-286 (*To*TCCP numbering; Fig. 1*B*), plus the "tandem" Cys sites, Cys-257 and Cys-258. Examination of eight tandem-Cys phytochrome sequences from glaucophytes currently present in publicly available databases also supports this hypothesis; all six signature positions for these TCEPs possess the same amino acids found in *To*TCCP, conservative amino acid substitutions, and/or variants present in one or more cyanobacterial TCCP representative (see Data File S1). Attempts to multiplex all of these TCCP-signature residues into the *Sy*Cph1 scaffold to secure a variant with a robust TCCP photocycle so far have been stymied by low yields of recombinant protein. Additional mutagenesis to sustain protein folding of *Sy*Cph1 and other phytochrome candidates may be needed.

A roadmap toward spectral diversification of plant phytochromes

Among the more exciting discoveries of this work is the generation of the C258S variant of *To*TCCP that has a G/R photocycle similar to RcaE. Although the same residue exchange in other TCCPs failed to generate variants with robust G/R photocycles, this suggests that it will be possible to generate variants of plant phytochromes with a broad range of photocycles, considerably extending their R/FR photosensory range. By introducing these variants into plant phyA or phyB photoreceptors, we hope to examine how changes in wavelength sensitivity will influence plant performance (49, 50). Such phytochrome variants could prove better than their WT counterparts for sustaining robust growth and development in artificial light environments that lack sufficient sunlight.

Toward the future, one pressing question left to address is the structural basis for FR-absorption of cyanobacterial and algal phytochromes that use PCB as chromophore precursor. Despite our efforts to reintroduce residues found in the chromophore-binding pockets of Cph1, Cph2, and algal phytochromes, we have yet to secure a variant of *To*TCCP whose photoproduct absorbs in the far-red. We believe that the cysteine variant C258H, which possesses a photoinactive R-absorbing dark-state, is a good place to start these investigations. By introducing other variant amino acid substitutions, both targeted and random, such studies are expected to provide valuable insight into the molecular basis of FR-absorption by plant, algal, and cyanobacterial phytochromes.

Experimental procedures

Expression and purification of recombinant His-tagged PCMs of TCCPs from BV-, PCB-, or PΦB-producing E. coli cultures

Plasmids pPL-BV, pPL-PCB, and pPL-PΦB were used for BV, PCB, and PΦB biosynthesis in *E. coli* (51). PCMs of TCCPs, *To*TCCP (Tpr0787, GenBank™ accession MG345012), *Sc*TCCP (Spr6403, GenBank™ accession MG345011), and *Gl*TCCP (Gpl2095, GenBank™ accession MG345010), were amplified by PCR with appropriate primers (Table S1) with genomic DNA from *Tolypothrix* PCC 7910, *Gloeocapsa* PCC 7513, and *Scytonema* PCC 10023 (axenic strains and genomic DNAs provided by M. Gugger, Collection of Cyanobacteria of the Institute Pasteur) as templates (52–54). PCR fragments were digested with appropriate restriction enzymes and then cloned into the pBAD-MycHisC vector (Invitrogen) to yield pBAD-TCCP^{PCM} bacterial expression plasmids for various TCCPs. All constructs were verified by oligonucleotide sequencing. *E. coli* LMG194 (Invitrogen) cells co-transformed with pBAD-TCCP^{PCM} and pPL-BV, -PCB, and -PΦB were grown overnight at 37 °C in 5 ml of minimal medium RM (55) containing 50 μg/ml of kanamycin and 200 μg/ml of ampicillin. Recombinant PCM proteins were isolated and further purified by nickel affinity chromatography (nickel-nitrilotriacetic acid resin; Qiagen) as previously described (52). Eluted proteins in elution buffer (50 mM Tris-HCl, pH 8, 300 mM NaCl, and 250 mM imidazole) were desalted and concentrated to yield a final concentration of 300 μM NaCl and 250 μM imidazole in 50 mM Tris-HCl buffer, pH 8, using an Amicon Ultra Centrifugal filter (Millipore). For pH titration and shift experiments, concentrated protein samples were washed twice by centrifugation with distilled water adjusted to pH 8 with NaOH. Both photostates of recombinant TCCPs were denatured by addition of a final concentration of 8 M urea-HCl, pH 2.0 (56), or 6 M guanidinium chloride, 0.1 M citrate, pH 2.2 (15), at room temperature in the dark.

Spectrophotometric analyses

Steady-state absorbance of purified TCCPs were recorded at room temperature with a UV1601 spectrophotometer (Shimadzu, Japan) in standard assay buffer (50 mM Tris-HCl, pH 8) or after dilution with buffers of varying pH from 5 to 11 as described below. Forward and reverse photointerconversions were triggered in the transparent tube using a UV-A tube (Model XX-40, Spectroline, 355 ± 28.6 nm) or blue or red LED lamps (Sungkwang LED Co., 525 ± 15 or 660 ± 15). Incident photon fluxes for UV-A (70 μW cm^{-2}), blue (52.8 μmol m^{-2} s^{-1}) and green (15.9 μmol m^{-2} s^{-1}) lights for forward and reverse photoconversions were illuminated for 1 min and dark 15*E* to 15*Z* reversion was undetectable for any sample.

pH titration assays

Fifteen μl of different buffers were added into transparent tubes containing 135 μl of the purified TCCP samples (about 2.8∼4.7 μg) in either the 15*Z* dark-state or 15*E* lit state after saturating irradiation with blue light. Buffers included 1 M MES-NaOH for pH 5 and 6; 1 M Tris-HCl for pH 7, 8, and 9; 1 M glycine-NaOH for pH 10 and 11; and 1 M KCl-NaOH for pH 12 and 13. After irradiation, all sample manipulations was performed in darkness. For pH-jump experiments, 30 μl of each protein sample in distilled water adjusted pH 8 was transferred to the tube containing 120 μl of the designated 1 M stock buffer. Spectra were recorded immediately after sample mixing by gentle pipetting (29). To estimate pK_a values for 15*E* *To*TCCP samples, the absorbance at 662 nm was plotted against the pH and then fitted to a hyperbolic equation (OriginPro 8.1) (57). pK_a values for other TCCP samples were determined similarly using appropriate irradiation wavelengths and peak absorbance.

SDS-PAGE and in-gel zinc-dependent fluorescence assays

For zinc in-gel fluorescence analysis (58), purified TCCPs (3 μg) were separated on a 12% (w/v) SDS-PAGE gel. Gels were then soaked in unbuffered 20 mM zinc acetate at room temperature for 30 min in the dark, and then imaged for fluorescence under UV-B excitation (302 nm) using a Bio-Rad Gel Doc 2000 equipped with a blue bandpass filter (480BP). Gels were stained with Coomassie Brilliant Blue R-250 (Bio-Rad) and reimaged to determine abundance of each polypeptide using a Bio-Rad ChemiDoc imager. Concentrations of thioether-bound 15*Z*-PCB and 15*Z*-PΦB were calculated after denaturation in 8 M urea adjusted to pH 2.0 with HCl using extinction coefficients of 35.5 mM^{-1} cm^{-1} at 663 nm (59, 60) and 32.1 mM^{-1} cm^{-1} at 660 nm (60, 61), respectively. Protein concentrations were then estimated on the denatured samples using the calculated molar extinction coefficient (ϵ) at 280 nm provided by the ExPASy ProtParam tool (RRID: SCR_018087) based on the His_6-tagged polypeptide sequences (*To*TCCP, 63,870 M^{-1} cm^{-1}; *Sc*TCCP, 56,880 M^{-1} cm^{-1}; and *Gl*TCCP, 59,735 M^{-1} cm^{-1}) and correcting for protein absorption at 280 nm. When expression levels were low, relative protein concentrations were determined using Bio-Rad's Quantity One™ software. Chromophorylation yields of acid-denatured TCCP samples were determined by dividing the concentration of the bilin by the concentration of the protein (62).

Bioinformatics and phylogenetic reconstructions

Phytochrome protein sequences *Sy*Cph1, *Ca*CphB/BphP, and *To*TCCP (Tpr0787) were used for BlastP analysis as query sequences and yielded 416 protein sequences from 174 cyanobacteria genomes and 85 protein sequences from 68 bacterial genomes ($E \leq 1 \times 10^{-7}$). For phylogenetic reconstructions, multiple amino acid sequence alignments were carried out using Clustal Omega (RRID: SCR_00159). For phylogenetic tree construction of cyanobacterial phytochromes we collected the submitted phytochrome-related sequences of bacteria, yeast, glaucophytes, and streptophytes from NCBI. We used the predicted PAS, GAF, and PHY domain sequences for reducing the discriminant disorder resulting from the interspecies variations of N-terminal sequences. A total of 172 amino acid sequences were involved in the dataset and aligned using ClustalW in MEGA7 (64). The maximum likelihood (ML) tree was constructed based on the best substitution model, which was selected the LG + Γ + I model (63) with γ distribution (5 categories; +Γ, parameter = 1.318) and invariable site (+I, 2.02% sites) in MEGA7 (64). The bootstrap value was estimated using

1,000 replicates with the same substitution model. Thick branches in the phylogenetic tree indicated >80% of the ML support value. Homology modeling of the PCM of *To*TCCP was performed online (RRID: SCR_018123) using default parameter settings and the 15*E* state of agp2-PAiRFP2 (6G1Z) as template.

Data availability

All the data are contained within the manuscript and the associated supporting information files. Proteins presented in this paper have been deposited in GenBank™ with IDs MG345010, MG345011, MG345012, and MG811563.

Author contributions—J.-Y. S. investigation; J.-Y. S., H. Y. L., and H. W. Y. methodology; J.-J. S. software; J.-J. S. visualization; J. C. L. and Y.-I. P. conceptualization; J. C. L. and Y.-I. P. supervision; J. C. L. and Y.-I. P. writing-review and editing; Y.-I. P. funding acquisition; Y.-I. P. writing-original draft.

Acknowledgments—We thank Dr. Nathan C. Rockwell for performing the phylogenetic analysis and Dr. Sung Mi Cho for helpful discussion.

References

1. Karniol, B., Wagner, J. R., Walker, J. M., and Vierstra, R. D. (2005) Phylogenetic analysis of the phytochrome superfamily reveals distinct microbial subfamilies of photoreceptors. *Biochem. J.* **392,** 103–116 CrossRef Medline
2. Rockwell, N. C., Su, Y. S., and Lagarias, J. C. (2006) Phytochrome structure and signaling mechanisms. *Annu. Rev. Plant Biol.* **57,** 837–858 CrossRef
3. Li, F. W., Melkonian, M., Rothfels, C. J., Villarreal, J. C., Stevenson, D. W., Graham, S. W., Wong, G. K., Pryer, K. M., and Mathews, S. (2015) Phytochrome diversity in green plants and the origin of canonical plant phytochromes. *Nat. Commun.* **6,** 7852 CrossRef Medline
4. Rockwell, N. C., and Lagarias, J. C. (2017) Phytochrome diversification in cyanobacteria and eukaryotic algae. *Curr. Opin. Plant. Biol.* **37,** 87–93 CrossRef Medline
5. Song, C., Psakis, G., Lang, C., Mailliet, J., Gärtner, W., Hughes, J., and Matysik, J. (2011) Two ground state isoforms and a chromophore D-ring photoflip triggering extensive intramolecular changes in a canonical phytochrome. *Proc. Natl. Acad. Sci. U.S.A.* **108,** 3842–3847 CrossRef Medline
6. Yang, X., Ren, Z., Kuk, J., and Moffat, K. (2011) Temperature-scan cryocrystallography reveals reaction intermediates in bacteriophytochrome. *Nature* **479,** 428–432 CrossRef Medline
7. Rockwell, N. C., and Lagarias, J. C. (2010) A brief history of phytochromes. *Chem. Phys. Chem.* **11,** 1172–1180 CrossRef Medline
8. Davis, S. J., Vener, A. V., and Vierstra, R. D. (1999) Bacteriophytochromes: phytochrome-like photoreceptors from nonphotosynthetic bacteria. *Science* **286,** 2517–2520 CrossRef Medline
9. Bhoo, S. H., Davis, S. J., Walker, J., Karniol, B., and Vierstra, R. D. (2001) Bacteriophytochromes are photochromic histidine kinases using a biliverdin chromophore. *Nature* **414,** 776–779 CrossRef Medline
10. Lamparter, T., Michael, N., Mittmann, F., and Esteban, B. (2002) Phytochrome from *Agrobacterium tumefaciens* has unusual spectral properties and reveals an N-terminal chromophore attachment site. *Proc. Natl. Acad. Sci. U.S.A.* **99,** 11628–11633 CrossRef Medline
11. Jorissen, H. J., Quest, B., Lindner, I., Tandeau de Marsac, N., and Gärtner, W. (2002) Phytochromes with noncovalently bound chromophores: the ability of apophytochromes to direct tetrapyrrole photoisomerization. *Photochem. Photobiol.* **75,** 554–559 CrossRef Medline
12. Giraud, E., Fardoux, J., Fourrier, N., Hannibal, L., Genty, B., Bouyer, P., Dreyfus, B., and Verméglio, A. (2002) Bacteriophytochrome controls photosystem synthesis in anoxygenic bacterial. *Nature* **417,** 202–205 CrossRef Medline
13. Tasler, R., Moises, T., and Frankenberg-Dinkel, N. (2005) Biochemical and spectroscopic characterization of the bacterial phytochrome of *Pseudomonas aeruginosa*. *FEBS J.* **272,** 1927–1936 CrossRef Medline
14. Fortunato, A. E., Jaubert, M., Enomoto, G., Bouly, J. P., Raniello, R., Thaler, M., Malviya, S., Bernardes, F., Rappaport, J. S., Gentili, B., Huysman, M. J., Carbone, A., Bowler, C., d'Alcalà, M. R., Ikeuchi, M., and Falciatore, A. (2016) Diatom phytochromes reveal the existence of far-red-light-based sensing in the ocean. *Plant Cell* **28,** 616–628 CrossRef Medline
15. Rockwell, N. C., Martin, S. S., Feoktistova, K., and Lagarias, J. C. (2011) Diverse two-cysteine photocycles in phytochromes and cyanobacteriochromes. *Proc. Natl. Acad. Sci. U.S.A.* **108,** 11854–11859 CrossRef Medline
16. Burgie, E. S., Walker, J. M., Phillips, G. N., Jr., and Vierstra, R. D. (2013) A photo-labile thioether linkage to phycoviolobilin provides the foundation for the blue/green photocycles in DXCF-cyanobacteriochromes. *Structure* **21,** 88–97 CrossRef Medline
17. Rockwell, N. C., Duanmu, D., Martin, S. S., Bachy, C., Price, D. C., Bhattacharya, D., Worden, A. Z., and Lagarias, J. C. (2014) Eukaryotic algal phytochromes span the visible spectrum. *Proc. Natl. Acad. Sci. U.S.A.* **111,** 3871–3876 CrossRef Medline
18. Rockwell, N. C., and Lagarias, J. C. (2020) Phytochrome evolution in 3D: Deletion, duplication, and diversification. *New Phytol.* **225,** 2283–2300 Medline
19. Rockwell, N. C., Njuguna, S. L., Roberts, L., Castillo, E., Parson, V. L., Dwojak, S., Lagarias, J. C., and Spiller, S. C. (2008) A second conserved GAF domain cysteine is required for the blue/green photoreversibility of cyanobacteriochrome Tlr0924 from *Thermosynechococcus elongatus*. *Biochemistry* **47,** 7304–7316 CrossRef Medline
20. Ishizuka, T., Kamiya, A., Suzuki, H., Narikawa, R., Noguchi, T., Kohchi, T., Inomata, K., and Ikeuchi, M. (2011) The cyanobacteriochrome, TePixJ, isomerizes its own chromophore by converting phycocyanobilin to phycoviolobilin. *Biochemistry* **50,** 953–961 CrossRef Medline
21. Enomoto, G., Hirose, Y., Narikawa, R., and Ikeuchi, M. (2012) Thiol-based photocycle of the blue and teal light-sensing cyanobacteriochrome Tlr1999. *Biochemistry* **51,** 3050–3058 CrossRef Medline
22. Narikawa, R., Ishizuka, T., Muraki, N., Shiba, T., Kurisu, G., and Ikeuchi, M. (2013) Structures of cyanobacteriochromes from phototaxis regulators AnPixJ and TePixJ reveal general and specific photoconversion mechanism. *Proc. Natl. Acad. Sci. U.S.A.* **110,** 918–923 CrossRef Medline
23. Narikawa, R., Enomoto, G., Win, N.-N., Fushimi, K., and Ikeuchi, M. (2014) A new type of dual-cys cyanobacteriochrome GAF domain found in cyanobacterium *Acaryochloris marina*, which has an unusual red/blue reversible photoconversion cycle. *Biochemistry* **53,** 5051–5059 CrossRef Medline
24. Cornilescu, C. C., Cornilescu, G., Burgie, E. S., Markley, J. L., Ulijasz, A. T., and Vierstra, R. D. (2014) Dynamic structural changes underpin photoconversion of a blue/green cyanobacteriochrome between its dark and photoactivated states. *J. Biol. Chem.* **289,** 3055–3065 CrossRef Medline
25. Hasegawa, M., Fushimi, K., Miyake, K., Nakajima, T., Oikawa, Y., Enomoto, G., Sato, M., Ikeuchi, M., and Narikawa, R. (2018) Molecular characterization of DXCF cyanobacteriochromes from the cyanobacterium *Acaryochloris marina* identifies a blue-light power sensor. *J. Biol. Chem.* **293,** 1713–1727 CrossRef Medline
26. Sato, T., Kikukawa, T., Miyoshi, R., Kajimoto, K., Yonekawa, C., Fujisawa, T., Unno, M., Eki, T., and Hirose, Y. (2019) Protochromic absorption changes in the two-cysteine photocycle of a blue/orange cyanobacteriochrome. *J. Biol. Chem.* **294,** 18909–18922 CrossRef Medline
27. West, A. H., and Stock, A. M. (2001) Histidine kinases and response regulator proteins in two-component signaling systems. *Trend. Biochem. Sci.* **26,** 369–376 CrossRef Medline
28. Essen, L. O., Mailliet, J., and Hughes, J. (2008) The structure of a complete phytochrome sensory module in the Pr ground state. *Proc. Natl. Acad. Sci. U.S.A.* **105,** 14709–14714 CrossRef Medline
29. Hirose, Y., Rockwell, N. C., Nishiyama, K., Narikawa, R., Ukaji, Y., Inomata, K., Lagarias, J. C., and Ikeuchi, M. (2013) Green/red cyanobacteriochromes regulate complementary chromatic acclimation via a protochromic photocycle. *Proc. Natl. Acad. Sci. U.S.A.* **110,** 4974–4979 CrossRef Medline

30. Anders, K., Daminelli-Widany, G., Mroginski, M. A., von Stetten, D., and Essen, L. O. (2013) Structure of the cyanobacterial phytochrome 2 photosensor implies a tryptophan switch for phytochrome signaling. *J. Biol. Chem.* **288,** 35714–35725 CrossRef Medline
31. Burgie, E. S., Bussell, A. N., Walker, J. M., Dubiel, K., and Vierstra, R. D. (2014) Crystal structure of the photosensing module from a red/far-red light-absorbing plant phytochrome. *Proc. Natl. Acad. Sci. U.S.A.* **111,** 10179–10184 CrossRef Medline
32. Wu, S. H., and Lagarias, J. C. (2000) Defining the bilin lyase domain: lessons from the extended phytochrome superfamily. *Biochemistry* **39,** 13487–13495 CrossRef Medline
33. Schirrmeister, B. E., de Vos, J. M., Antonellic, A., and Bagheri, H. C. (2013) Evolution of multicellularity coincided with increased diversification of cyanobacteria and the Great Oxidation Event. *Proc. Natl. Acad. Sci. U.S.A.* **110,** 1791–1796 CrossRef Medline
34. Adams, D. G. (1997) Cyanobacteria. in *Bacteria as Multicellular Organisms* (Shapiro, J., and Dworkin, M., eds) pp. 109–148, Oxford University Press, New York
35. Falk, H. (1989) *The Chemistry of Linear Oligopyrroles and Bile Pigments*, pp. 621, Springer-Verlag, Vienna
36. Burgie, E. S., Clinger, J. A., Miller, M. D., Brewster, A. S., Aller, P., Butryn, A., Fuller, F. D., Gul, S., Young, I. D., Pham, C. C., Kim, I. S., Bhowmick, A., O'Riordan, L. J., Sutherlin, K. D., Heinemann, J. V., *et al.* (2020) Photoreversible interconversion of a phytochrome photosensory module in the crystalline state. *Proc. Natl. Acad. Sci. U.S.A.* **117,** 300–307 CrossRef Medline
37. Wagner, J. R., Zhang, J., Brunzelle, J. S., Vierstra, R. D., and Forest, K. T. (2007) High resolution structure of *Deinococcus* bacteriophytochrome yields new insights into phytochrome architecture and evolution. *J. Biol. Chem.* **282,** 12298–12309 CrossRef Medline
38. Shang, L., Rockwell, N. C., Martin, S. S., and Lagarias, J. C. (2010) Biliverdin amides reveal roles for propionate side chains in bilin reductase recognition and in holophytochrome assembly and photoconversion. *Biochemistry* **49,** 6070–6082 CrossRef Medline
39. Rockwell, N. C., Martin, S. S., Gulevich, A. G., and Lagarias, J. C. (2012) Phycoviolobilin formation and spectral tuning in the DXCF cyanobacteriochrome subfamily. *Biochemistry* **51,** 1449–1463 CrossRef Medline
40. Lim, S., Yu, Q., Gottlieb, S. M., Chang, C.-W., Rockwell, N. C., Martin, S. S., Madsen, D., Lagarias, J. C., Larsen, D. S., and Ames, J. B. (2018) Correlating structural and photochemical heterogeneity in cyanobacteriochrome NpR6012g4. *Proc. Natl. Acad. Sci. U.S.A.* **115,** 4387–4392 CrossRef Medline
41. Buhrke, D., Battocchio, G., Wilkening, S., Blain-Hartung, M., Baumann, T., Schmitt, F. J., Friedrich, T., Mroginski, M. A., and Hildebrandt, P. (2020) Red, orange, green: light- and temperature-dependent color tuning in a cyanobacteriochrome. *Biochemistry* **59,** 509–519 CrossRef Medline
42. Yang, X., Kuk, J., and Moffat, K. (2008) Crystal structure of *Pseudomonas aeruginosa* bacteriophytochrome: photoconversion and signal transduction. *Proc. Natl. Acad. Sci. U.S.A.* **105,** 14715–14720 CrossRef Medline
43. Schmidt, A., Sauthof, L., Szczepek, M., Lopez, M. F., Escobar, F. V., Qureshi, B. M., Michael, N., Buhrke, D., Stevens, T., Kwiatkowski, D., von Stetten, D., Mroginski, M. A., Krauβ, N., Lamparter, T., Hildebrandt, P., and Scheerer, P. (2018) Structural snapshot of a bacterial phytochrome in its functional intermediate state. *Nat. Commun.* **9,** 4912 CrossRef Medline
44. Kim, P. W., Rockwell, N. C., Martin, S. S., Lagarias, J. C., and Larsen, D. S. (2014) Dynamic inhomogeneity in the photodynamics of cyanobacterial phytochrome Cph1. *Biochemistry* **53,** 2818–2826 CrossRef Medline
45. Kim, P. W., Rockwell, N. C., Martin, S. S., Lagarias, J. C., and Larsen, D. S. (2014) Heterogeneous photodynamics of the Pfr state in the cyanobacterial phytochrome Cph1. *Biochemistry* **53,** 4601–4611 CrossRef Medline
46. Velazquez-Escobar, F., Lang, C., Takiden, A., Schneider, C., Balke, J., Hughes, J., Alexiev, U., Hildebrandt, P., and Mroginski, M. A. (2017) Protonation-dependent structural heterogeneity in the chromophore binding site of cyanobacterial phytochrome Cph1. *J. Phys. Chem. B* **121,** 47–57 CrossRef Medline
47. Kirpich, J., Mix, L. T., Martin, S. S., Rockwell, N. C., Lagarias, J. C., and Larsen, D. S. (2018) Protonation heterogeneity modulates the ultrafast photocycle initiation dynamics of phytochrome Cph1. *J. Phys. Chem. Lett.* **9,** 3454–3462 CrossRef
48. Takala, H., Björling, A., Berntsson, O., Lehtivuori, H., Niebling, S., Hoernke, M., Kosheleva, I., Henning, R., Menzel, A., Ihalainen, J. A., and Westenhoff, S. (2014) Signal amplification and transduction in phytochrome photosensors. *Nature* **509,** 245–248 CrossRef Medline
49. Zhang, J., Stankey, R. J., and Vierstra, R. D. (2013) Structure-guided engineering of plant phytochrome B with altered photochemistry and light signaling. *Plant Physiol.* **161,** 1445–1457 CrossRef Medline
50. Su, Y. S., and Lagarias, J. C. (2007) Light-independent phytochrome signalling mediated by dominant GAF domain tyrosine mutants of *Arabidopsis* phytochromes in transgenic plants. *Plant Cell* **19,** 2124–2139 CrossRef Medline
51. Fischer, A. J., Rockwell, N. C., Jang, A. Y., Ernst, L. A., Waggoner, A. S., Duan, Y., Lei, H., and Lagarias, J. C. (2005) Multiple roles of a conserved GAF domain tyrosine residue in cyanobacterial and plant phytochromes. *Biochemistry* **44,** 15203–15215 CrossRef Medline
52. Song, J. Y., Cho, H. S., Cho, J. I., Jeon, J. S., Lagarias, J. C., and Park, Y.-I. (2011b) A near ultraviolet cyanobacteriochrome signaling system promotes negative phototaxis in the cyanobacterium *Synechocystis* sp. PCC 6803. *Proc. Natl. Acad. Sci. U.S.A.* **108,** 10780–10785 CrossRef Medline
53. Cho, S. M., Jeoung, S. C., Song, J. Y., Kupriyanova, E. V., Pronina, N. A., Lee, B. W., Jo, S. W., Park, B. S., Choi, S. B., Song, J. J., and Park, Y.-I. (2015) Genomic survey and biochemical analysis of recombinant candidate cyanobacteriochromes reveals enrichment for near UV/violet sensors in the halotolerant and alkaliphilic cyanobacterium Microcoleus IPPAS B353. *J. Biol. Chem.* **290,** 28502–28514 CrossRef Medline
54. Cho, S. M., Jeoung, S. C., Song, J. Y., Song, J. J., and Park, Y.-I. (2017) Hydrophobic residues near the bilin chromophore-binding pocket modulates spectral tuning of insert-Cys subfamily of cyanobacteriochromes. *Sci. Rep.* **7,** 40576 CrossRef Medline
55. Gambetta, G. A., and Lagarias, J. C. (2001) Genetic engineering of phytochrome biosynthesis in bacteria. *Proc. Natl. Acad. Sci. U.S.A.* **98,** 10566–10571 CrossRef Medline
56. Ishizuka, T., Narikawa, R., Kohchi, T., Katayama, M., and Ikeuchi, M. (2007) Cyanobacteriochrome TePixJ of *Thermosynechococcus elongatus* harbors phycoviolobilin as a chromophore. *Plant Cell Physiol.* **48,** 1385–1390 CrossRef Medline
57. Zienicke, B., Molina, I., Glenz, R., Singer, P., Ehmer, D., Escobar, F. V., Hilderbrandt, P., Diller, R., and Lamparter, T. (2103) Unusual spectral properties of bacteriophytochrome Agp2 results from a deprotonation of the chromophore in the red-absorbing from Pr. *J. Biol. Chem.* **288,** 31738–31751 CrossRef Medline
58. Berkelman, T. R., and Lagarias, J. C. (1986) Visualization of bilin-linked peptides and proteins in polyacrylamide gels. *Anal. Biochem.* **156,** 194–201 CrossRef Medline
59. Glazer, A. N., and Fang, S. (1973) Chromophore content of blue-green algal phycobiliproteins. *J. Biol. Chem.* **248,** 659–662 Medline
60. Zhao, K. H., Porra, R. J., and Scheer, H. (2012) Phycobiliproteins. in *Handbook of Porphyrin Science* (Kadish, K., Guilard, R., and Smith, K., eds) Vol. 22, pp. 1–66, World Scientific, Singapore
61. Brandlmeier, T., Scheer, H., and Rudiger, W. (1981) Chromophore content and molar absorptivity of phytochrome in the Pr form. *Z. Naturforsch.* **36C,** 431–439 CrossRef
62. Biswas, A., Boutaghou, M. N., Alvey, R. M., Kronfel, C. M., Cole, R. B., Bryant, D. A., and Schluchter, W. M. (2011) Characterization of the activities of the CpeY, CpeZ, and CpeS bilin lyases in phycoerythrin biosynthesis in *Fremyella diplosiphon* strain UTEX 481. *J. Biol. Chem.* **286,** 35509–35521 CrossRef Medline
63. Le, S. Q., and Gascuel, O. (2008) An improved general amino acid replacement matrix. *Mol. Biol. Evol.* **25,** 1307–1320 CrossRef Medline
64. Kumar, S., Stecher, G., and Tamura, K. (2016) MEGA7: molecular evolutionary genetics analysis version 7.0 for bigger datasets. *Mol. Biol. Evol.* **33,** 1870–1874 CrossRef Medline